Fermi National Accelerator Laboratory

FERMILAB-Pub-94/240

A Scintillating Tile/Fiber System for the CDF Plug Upgrade EM Calorimeter

S. Aota, T. Asakawa, K. Hara, E. Hayashi, S. Kim,
K. Kondo, T. Kuwabara, S. Miyashita, H. Nakada, I. Nakano,
Y. Seiya, K. Takikawa, H. Toyoda, T. Uchida, K. Yasuoka

Institute of Physics, University of Tsukuba
Tennohdai 1-1-1, Tsukuba, Ibaraki, 305, Japan

M. Mishina

National Laboratory for High Energy Physics, KEK
Oho 1-1, Tsukuba, Ibaraki, 305, Japan

J. Iwai

Science and Engineering Research Laboratory, Waseda University
Kikui 17, Shinjuku-ku, Tokyo, 162, Japan

M. G. Albrow, J. Freeman, P. J. Limon

Fermi National Accelerator Laboratory
P.O.Box 500, Batavia, Illinois 60510, U.S.A.

August 1994

Submitted to *Nuclear Instruments and Methods.*

Operated by Universities Research Association Inc. under Contract No. DE-AC02-76CHO3000 with the United States Department of Energy

Disclaimer

A Scintillating Tile/Fiber System for the CDF Plug Upgrade EM Calorimeter

S. Aota, T. Asakawa, K. Hara, E. Hayashi, S. Kim,
K. Kondo, T. Kuwabara, S. Miyashita, H. Nakada, I. Nakano,
Y. Seiya, K. Takikawa, H. Toyoda, T. Uchida, K. Yasuoka

Institute of Physics, University of Tsukuba
Tennohdai 1-1-1, Tsukuba, Ibaraki, 305, Japan

M. Mishina

National Laboratory for High Energy Physics, KEK
Oho 1-1, Tsukuba, Ibaraki, 305, Japan

J. Iwai

Science and Engineering Research Laboratory, Waseda University
Kikui 17, Shinjuku-ku, Tokyo, 162, Japan

M. G. Albrow, J. Freeman, P. J. Limon

Fermi National Accelerator Laboratory
P.O.Box 500, Batavia, Illinois 60510, U.S.A.

Abstract

The medium angle plug calorimeter of the Collider Detector at Fermilab will be upgraded, replacing the existing gas calorimeter by a scintillating tile/fiber calorimeter. We describe the results of studies leading to the final design of the tile/fiber system. Kuraray SCSN38, Kuraray Y11 and PET film (E65) were chosen as materials for scintillating tiles, wavelength-shifting fibers and surface reflector on tiles, respectively, giving large light yield and uniform response. We optimized the fiber groove path in the tiles, groove cross sectional shape and depth for uniform response.

For the final design the average light yield exceeded 3.0 photoelectrons per minimum ionizing particle, the response non-uniformity in a tile was less than 2.5 % and the total cross-talk from a tile to the adjacent tiles was less than 2.0 %. These results satisfied our requirements.

Contents

1 Introduction

The CDF plug calorimeter [1] will be upgraded [2] in 1996, replacing the existing gas proportional chamber sampling calorimeter. We require the new calorimeter to have a fast response and minimal dead area. These properties can be achieved [3] using layers of scintillating tiles as the active medium, read out by wavelength-shifting plastic fibers embedded in grooves [4]. The WLS fibers are connected to clear fibers which transport the light to arrays of photomultipliers mounted at the back of the calorimeter. The new calorimeter consists of an electromagnetic section and a hadronic section. We have chosen materials and design features for the tile/fiber system in the EM section of the new calorimeter.

The tile/fiber EM calorimeter is a lead/scintillator sampling device and covers polar angles from 3° to 38°. It consists of 23 layers of 4 mm scintillator sheets and 4.5 mm lead plates clad with 0.5 mm stainless steel.

Each layer of the tile/fiber system is divided into 24 units, each covering an azimuthal angle of 15° as shown in Fig. 1. A 15° unit consists of 20 tiles for the 1st to 15th layers and 18 tiles for the 16th to 23rd layers. The scintillator is sandwiched between reflectors and top and bottom plastic plates, held together with plastic pins made of scintillating material at two diagonal corners of each tile. The top plate has a slit for each tile through which a WLS fiber spliced to a clear fiber enters a groove in the tile. Grooves are machined on the top plate to guide the clear fibers to two fiber connectors near the outer circumference of the calorimeter. Two tubes for radioactive sources were fixed in grooves in the top plate, passing through the centers of all tiles. We will calibrate the gain of each tile/fiber by moving ^{137}Cs γ-ray sources through these source tubes.

2 The Requirements for the CDF Plug Upgrade EM Calorimeter

The energy resolution of the calorimeter is given by:

$$(\frac{\sigma}{E})^2 = (\frac{\sigma_A}{\sqrt{E(GeV)}})^2 + (\sigma_B)^2 \quad (1)$$

The first term comes from sampling fluctuations and photostatistics. The sampling fluctuation coefficient (σ_A) with 4.5 mm lead plates is 14 %. The second term comes mainly from response non-uniformity of tiles within a tower. The requirements for the plug upgrade EM calorimeter were that the stochastic term σ_A should be less than 16 % and the constant term σ_B should be less than 1 %. Non-linearity of the calorimeter was required to be less than 1% in the energy range between 10 GeV and 400 GeV. In order to fulfill these criteria we required that the light yield be more than 3.0 photoelectrons/tile per minimum ionizing particle and the response non-uniformity in a tile be less than 2.5% [5].

We expect a maximum radiation dose of 500 krad/10 years at $\theta = 3°$ in the plug EM calorimeter near the shower maximum, and the material of the tile/fiber system should be radiation-hard to that level. We require that the decrease in light yield from the scintillator should be less than 15 % and the decrease in its attenuation length should be less than 30 % for the above maximum dose.

Optical cross-talk in a 15° unit degrades the energy resolution. We require that the total light cross-talk from a tile to all the adjacent tiles should be less than 3.5 %.

3 Light Yield Measurement

3.1 Experimental setup

We evaluated the light yield in terms of the number of photoelectrons produced in a PMT. The experimental setup for this measurement is shown in Fig. 2. We excited scintillator tiles with a ^{90}Sr β-ray source. The source had a collimator 5 mm in diameter and a trigger scintillator 2 mm in diameter was placed beneath the tile. The WLS fiber was coupled to the PMT with silicon grease for good reproducibility of the measurements. We used two types of PMT, Hamamatsu R329(H1161)[1] and R580-17[2]. The signal was digitized using a LeCroy 2249A CAMAC ADC module, and read out with an NEC PC-9801 personal computer.

3.2 Light yield

The average number of photoelectrons was calculated for PMT pulse-height distributions with typically 3000 events. The pulse-height distribution is a smeared Poisson distribution. The average number of photoelectrons can be determined from the pulse-height distribution once we know the pulse height for a single photoelectron.

The pulse height for a single photoelectron was measured with the same experimental setup by reducing the light intensity by insertion of neutral-density filters (with a typical transmission of 2%) between the WLS fiber and the PMT. Figure 3 shows a typical pulse-height distribution for this measurement, the peak around 43 ADC counts corresponding to a single photoelectron. The contribution from events with two or more photoelectrons is negligible. In order to determine the peak position precisely, we fit the distribution near the peak with a single Gaussian function, shown in the figure as a curve.

The next step was to determine the average number of photoelectrons in a given pulse-height distribution knowing the single photoelectron peak position. A typical pulse-height distribution is shown in Fig. 4. We tried two different methods for the determination of the light yield. The first method simply uses the average value of the

[1]The R329 photomultiplier tube has the same type of photocathode as the R580, which was used for the CDF central electromagnetic calorimeter, but has more dynode stages and thus a higher gain. An assembly of R329 and the base is called H1161

[2]The R580-17 is a green extended PMT which has a typically 15 % higher quantum efficiency at a wavelength around 500 nm than the R580.

pulse-height distribution divided by the single photoelectron peak position. The second method fits the distribution with a smeared Poisson distribution where the position and the width of a single photoelectron peak are fixed by the previous measurement. The fitted curve for the pulse-height distribution is also shown in Fig. 4. The results from the two methods agree well with each other: the difference is usually smaller than the statistical precision of the measurements. In the remainder of this paper, we use the first method.

We take enough events that the statistical error is less than 1.0%. The light yield of one sample tile/fiber has been measured several times to test the reproducibility of the measurement. Variations were less than 0.5%. .

3.3 Response uniformity

We measured the response of tile/fibers using a ^{90}Sr β-ray source. We used an automatic scanning system that positioned the source with an accuracy better than 50 μm to measure the response uniformity. In this setup, the source and a trigger counter were fixed, and a sample tile was moved in two-dimensions. The trigger counter under the sample tile consisted of a 2 mm diameter scintillator, a light guide, and a PMT. Since the β-ray source was disk-shaped with an active region 1 cm in diameter, we used a 5 mm diameter lead collimator. The PMT used in this measurement was an R329(H1161). We measured responses at 100 uniformly distributed points on a tile. Their r.m.s. variation was used as a measure of the non-uniformity.

4 Determination of Materials for the Tile/Fiber System

In this section we will discuss how we selected the scintillator, WLS fiber and reflector materials. The performance of a scintillating pin as a structural component of the tile/fiber system is also described.

4.1 Choice of scintillator and WLS fiber

We had several kinds of scintillators and WLS fibers as candidate materials for the tile/fiber system and we measured the light yield with various combinations. Samples of scintillators and WLS fibers are listed in Table 1. Tiles were 120 mm square and 4 mm thick. All tiles had a circular fiber groove with a radius of 57 mm, 2.1 mm deep and 1.1 mm wide. The four edges of sample tiles were painted white with NE650 white paint containing TiO_2. Two turns of Y11 fiber were embedded in each tile. We wrapped each sample with aluminized mylar. A ^{90}Sr β -ray source was put on the center of the sample. The trigger scintillator was 6 mm in diameter, fixed beneath the sample tile. We took 3,000 events for each sample; the results of these measurements are shown in Fig. 5. Scintillating tiles of SCSN38, SCSN38C, SCSN38D and BC408 gave significantly larger light yield than the others with the same WLS fiber. The WLS fibers of Kuraray Y11 and BCF91A which were made of the same materials showed larger light yields than the other WLS fibers.

		Sample Scintillators							
Kuraray	SCSN81:	S1	S2	S3	S4	S7	S8	S9	S14
	SCSN38:	38	38C'	38D'	S6	S13			
	SCSN88:	S10	S11	S12	S15	S16			
BICRON		BC408							
		Sample Wavelength-Shifting Fibers							
Kuraray		Y11		Y7		B2			
BICRON		BCF91A							

Table 1: Sample Scintillators and Fibers

We chose Kuraray SCSN38 and Y11 as materials for the scintillating tile and wavelength shifting fiber after competitive bidding.

4.2 Choice of reflector

We measured the light yield and response uniformity of tile/fibers with various reflector materials on the tile surfaces. The scintillating tile was SCSN38, 120 mm square and 4mm thick. Figure 6 shows the path of the fiber groove in a tile. The groove passed 5 mm from the tile edges and had a radius of 30 mm at the corners, and was 0.9 mm deep and 1.1 mm wide. The four edges of the tile were painted white. One-turn of Y11 fiber spliced to a 3 m clear fiber was embedded in the tile. We put a sample reflector on the top and bottom surfaces of the tile and wrapped it with aluminized mylar. The sample reflectors are listed in Table 2. We scanned a tile/fiber with a ^{90}Sr β-ray source with several reflectors at 100 uniformly-distributed points. The sample reflectors were a fiber paper, a PET film (E65) and an aluminized mylar. The diameter of the source collimator was 5 mm for this scan.

The results of the measurements are listed in Tables 2 and 3. The fiber paper and the PET film (E65) gave larger light yield than the others. The PET film (E65) gave the best response uniformity among the three samples. From these results we selected the PET film (E65) as the reflector on the tile surfaces.

4.3 Scintillating pin

A 15° unit consists of 20 tiles. The tiles have to be positioned in the unit with good precision. We used pins to fix the tiles and reflectors to the top and bottom plates. We developed scintillating pins to minimize the non-uniformity of the response around the pins. Two scintillating pins were used per tile at points 10 mm from the tile corners along a diagonal. We made the pin positions in the odd layers different from those in the even layers. The pin was 6.5 mm long and 3 mm in diameter as shown in Fig. 1.

We used the same sample of tile/fiber and the same experimental setup as described in the last subsection to measure the response around the scintillating pin, changing

Sample reflector	Light Yield (# of Photoelectrons)	Ratio
Fiber paper	4.31 ± 0.08	1.00
PET film (E65)	4.30 ± 0.08	0.99
PET film (E63)	4.21 ± 0.08	0.98
PET film (50)	4.03 ± 0.08	0.94
PET film (100)	3.90 ± 0.07	0.90
Aluminized mylar (thin)	3.90 ± 0.07	0.90
Aluminized mylar (thick)	3.82 ± 0.07	0.89
Aluminum foil	3.81 ± 0.07	0.88
Printer Paper	3.71 ± 0.07	0.86

Table 2: Light yield from tile/fiber with various reflectors

Sample	Response non-uniformity (%)
Fiber paper	2.22 ± 0.13
PET film (E65)	2.05 ± 0.12
Aluminized mylar	2.31 ± 0.14

Table 3: Response non-uniformity versus reflector materials

only the sizes of the collimator and trigger scintillator to 2 mm in diameter. We compare the result for the scintillating pin with that for a non-scintillating acrylic pin in Fig. 7. The scintillating pin recovers up to 50 % of the light yield. The modest recovery could be attributed to poor transmission at the pin surface, and we investigated two ways to improve this. The first is to coat the surface of the pin with an acrylic resin; results are also shown in Fig. 7. The response around the pin improved to 80 % . The second way is to increase the scintillator concentration. We measured the response for a scintillating pin that had 1.5 times the usual concentration and found that it did not show any improvement. This is because the concentration was already optimized so that the light yield from the pin saturated. To estimate the response on the scintillating pin, we used a simple model where the response on and off the pin was uniform, respectively, and the β-rays spread in the form of two-dimensional Gaussian. We found the sigma of the Gaussian to be 2.2 mm using data for a non-scintillating acrylic pin. The unsmeared response on the scintillating pin normalized to that off the pin was found to be 75 % .

We simulated the effect of this decrease in the response around the pin for 100 GeV electrons with GEANT Monte Carlo simulation. The response to electrons at the center of the pin normalized to that on the tile center is 0.988, effectively eliminating non-uniformity caused by the pins.

We checked the stability of the scintillating pin by a heat-cycle test, with a heat-cycle pattern shown in Fig. 8. The temperature changed from $-20.0°$C to $+50.0°$C at a rate of 1 cycle per day for six days. This pattern is based on an industrial standard. Figure 9 shows the response on the pin before the heat cycle, after 3 heat cycles and 6 heat cycles. We did not see any significant differences between the responses before and after the heat cycles.

5 Radiation-Hardness Test of Scintillators

We estimate that scintillating tiles in the CDF plug upgrade EM calorimeter will be irradiated to a dose of 500 krad in 10 years at $\theta = 3°$. We require that the decrease in light yield of the scintillator should be less than 15% and the decrease in attenuation length should be less than 30% at this dose. Sample scintillators SCSN81, SCSN38D and BC408 were irradiated by ^{60}Co γ-rays up to total doses of 0.5 Mrad and 1.0 Mrad and we measured the light yield and attenuation length of scintillators before and after irradiation.

5.1 Light yield

We used 30-mm-square 4-mm-thick scintillator tiles to measure the scintillator light yield. We put black tape on the side surfaces except for one side attached to a PMT (Hamamatsu H1161) to exclude the contribution of reflected light. The other surfaces were wrapped with paper. We put a neutral-density filter with transmission of 10 % between the sample scintillator block and the PMT. A β-ray ^{90}Sr source was put on a 3 mm diameter, 5 mm thick lead collimator. A trigger counter was put underneath the scintillator block as shown in Fig. 10. The light yield after the

irradiation normalized to that before the irradiation is listed in Table 4. All scintillators satisfied our requirements.

Sample scintillator	before Light yield(N_{pe})	after 0.5 Mrad Decrease in light	1.0 Mrad yield(%)
SCSN81	9.14 ± 0.14	2.2 ± 0.1	8.0 ± 0.2
SCSN38D	10.46 ± 0.14	5.6 ± 0.1	13.6 ± 0.3
BC408	8.95 ± 0.13	8.1 ± 0.2	14.6 ± 0.4

Table 4: Light yield of scintillator vs. dose

5.2 Attenuation length

We used scintillators in the form of a bar to measure attenuation lengths. The samples were 200 mm long, 20 mm wide and 4 mm thick. We put black tape on the side surfaces except for one end attached to a PMT. The other surfaces are wrapped with paper as in the light yield measurement. We scanned sample scintillating bars along the center line at points 2 cm, 4 cm, 7 cm, 10 cm, 14 cm, and 18 cm away from the PMT with a ^{90}Sr source β-ray as shown in Fig. 11. We obtained an attenuation curve from one scan. We fitted the curve with the following exponential function and obtained an attenuation length λ:

$$F(x) = Ne^{-\frac{x}{\lambda}}. \tag{2}$$

The attenuation lengths after the irradiation normalized to that before the irradiation are summarized in Table 5. SCSN38D has the best radiation hardness in attenuation length and satisfies our requirements.

Sample scintillator	before Attenuation length (mm)	after 0.5 Mrad Decrease in attenuation length	1.0 Mrad (%)
SCSN81	648 ± 43	32 ± 2	41 ± 3
SCSN38D	402 ± 20	16 ± 1	29 ± 2
BC408	644 ± 12	31 ± 2	32 ± 2

Table 5: Attenuation length vs. dose

6 Response Uniformity vs. Groove Design

We determined the best groove design with a view to obtaining a uniform response. In this section we describe our studies of the groove design.

6.1 Groove path in a tile

The response uniformity depends on the groove path in a tile, and we scanned tiles with various groove paths to determine this dependence. We used sample tiles with two sizes and several groove paths. The sample tiles were SCSN38 and their edges were painted white with BICRON BC-600 paint. Six kinds of tiles were used. Four tiles were 200 mm square and 4 mm thick. Two were 120 mm square and 4 mm thick. The basic groove pattern is a square with rounded corners. We made four geometries A(200), B(200), C(200) and D(200) for the 200-mm-square tiles, the straight part of the grooves being 5 mm from the tile edges and the groove radii at the corners being 30 mm, 50 mm, 70 mm and 95 mm. We made two groove paths, A(120) and B(120) for the 120-mm-square tiles, 5 mm from the edges with groove radii of 30 mm and 55 mm. We embedded a Y11 WLS fiber spliced to a 3 m clear fiber in the sample tiles, and put PET (E65) films on the both surfaces of the tiles. We wrapped the whole samples with aluminized mylar. We scanned these samples at 100 uniformly distributed points for the 120-mm-square tiles and at 400 points for the 200-mm-square tiles. We took 3,000 events at each point to keep statistical errors less than 1.0 %.

The response maps of these scans are shown in Figs. 12 and 13. Among the 200-mm-square tiles, B(200) and C(200) gave a more uniform response than the others. The tile A(200) had low response around the tile corners and the tile D(200) had low response around the tile center. For the 120-mm-square tiles, A(120) showed more uniform response than B(120), the tile B(120) having low response at the tile corners. The typical size of the real tiles in the CDF plug upgrade EM calorimeter is about 100 mm square. Since the minimum safe fiber bending radius was 25 mm [6], we chose 30 mm as the groove radius at the tile corners.

6.2 Groove cross sectional shape

Grooves with keyhole cross sectional shape hold the fibers in the grooves. We made tiles with four types of keyhole shape grooves to examine the dependence of the response uniformity on the groove cross sectional shape. All tiles were made of SCSN38 and were 120 mm square and 4 mm thick. The grooves passed 5 mm from tile edges and the radius of the grooves at the tile corners was 30 mm. The grooves were 1.8 mm deep and 0.9 mm wide. The groove cross sectional shapes of four samples are shown in Fig. 14. We embedded a Y11 WLS fiber spliced to a 3 m clear fiber in a sample tile, put PET (E65) films on the tile surfaces as a reflector, painted the tile sides white, and wrapped the whole sample with aluminized mylar. We scanned the sample at 100 points to obtain the response uniformity. The results of these measurements for all samples are summarized in Table 6. We did not see any significant difference in the response uniformity among the four samples, all types satisfying our requirements. We selected the type D groove shape.

Keyhole Groove Shape	Type A	B	C	D
Non-uniformity (%)	2.20 ± 0.14	2.12 ± 0.14	2.18 ± 0.14	2.08 ± 0.13

Table 6: Response non-uniformity vs. groove cross sectional shape

6.3 Groove depth

The response around the fiber changes rapidly. Scanning a tile along a diagonal line, the response increases near the groove and decreases just on the groove as shown in Fig. 15. We made seven kinds of tiles to examine the dependence of the response uniformity on the groove depth. Sample tiles were SCSN38, 120 mm square and 4mm thick. The groove passed 5 mm from the tile edges with a 30 mm radius at the corners. The groove depth was varied from 1.2 mm to 2.3 mm. We embedded a Y11 fiber in the groove and wrapped the sample with aluminized mylar. We scanned all sample tiles to measure the response uniformity on and off the fiber groove. The scanned points on the groove are shown in Fig. 16 with circles.

The results are shown in Fig. 17. The upper figure shows the average response on the groove vs. groove depth, normalized to the average response off the groove. For the tile with a 1.2-mm-deep groove, the response on the groove was larger than that off the groove by 5%. The response decreased linearly as a function of the groove depth at a rate of -1.0% per 0.1 mm. When the depth was around 1.8 mm, the average response on the groove became equal that off the groove. The lower figure shows the response non-uniformity vs. the groove depth. For depths between 1.6 mm and 1.9 mm the non-uniformity had a minimum value around 2.0 %. Thus the groove depth was chosen to be 1.7 mm for a 120-mm-square tile.

6.4 Groove depth optimization for the real-shape tiles

We measured the response uniformity for tiles of the correct shape for the plug upgrade EM calorimeter. A 15° unit has twenty tiles in twelve approximately trapezoidal shapes as shown in Fig. 18. We made twelve tiles in the shape of the 12th layer of a 15° unit. The groove had the D-type keyhole shape, passed 5 mm from the tile edges, was 30 mm in radius at the corners and 1.7 mm deep. We measured the response uniformity of these tiles, listing the results in Table 7; the response map of tile No.18 is shown in Fig. 19.

The larger and smaller tiles gave less uniform response than the middle-size tiles. The relative response around the grooves varied as a function of the side length of the tile. For the tiles with a longer side length, the response near the side became relatively larger, as shown in Fig. 20. The plot was fitted with a Fermi distribution function (3), P_1, P_2 and P_3 being the fitting parameters.

The average response on the groove varied as a function of the groove depth at a rate of -1.0 % per 0.1 mm as mentioned before. Using the Fermi distribution function

Tile Number	Response Non-Uniformity (%)
1	6.31 ± 0.36
2	3.14 ± 0.18
3	2.19 ± 0.12
4	1.80 ± 0.11
8	2.57 ± 0.15
10	2.31 ± 0.14
12	2.52 ± 0.15
14	1.95 ± 0.11
16	2.92 ± 0.17
18	3.27 ± 0.20
20	3.89 ± 0.23

Table 7: The response non-uniformity of tiles in a 15° unit with the groove depth of 1.7 mm

and this rate, we optimized the groove depth for tiles of the correct shape. For the side length of L mm, the relative response near the side of the tile, Y(L) %, was calculated with the Fermi distribution function:

$$\begin{aligned} Y(L) &= \frac{2P_1}{1+e^{-P_2(L-P_3)}} - P_1 \qquad (3) \\ P_1 &= 4.93 \\ P_2 &= 0.0850 \\ P_3 &= 97.8 \end{aligned}$$

To decrease the response by Y%, we have to make the groove deeper by $0.1\times$ Y mm. We calculated the optimum groove depths for each side of all tiles by this algorithm. As one tile had four side (or arc) lengths, we obtained four values and we calculated a weighted mean for each tile, using that as the groove depth for that tile. The final values varied from 1.5 mm to 2.2 mm depending on the tile size.

For No.19 and No.20 tiles in the 12th, 13th, 14th and 15th layers, we did not take the average of the four optimum depths but kept different groove depths for the sides and arcs, the sides being much shorter than the arcs.

7 Fiber

7.1 Fiber fabrication

WLS fiber ends were mirrored by aluminum sputtering, and coated with MgF_2 to protect the mirror end. Mirroring methods of aluminum vapor deposition and white

paint were also tried and were found to give about 80% more light than a sample with the end painted black, while aluminum sputtering showed an 89% increase.

WLS fiber and clear fiber are bonded by a method based on thermal fusion [7]. This method was improved using PEEK tube which aligned two fiber axes before splicing and supported the fused joint mechanically after splicing [6].

7.2 Multiclad fiber

The measurements described so far were performed with single-clad fibers. Multiclad fibers invented by Kuraray have a core, inner cladding and outer cladding. Refractive indices of the core, inner and outer cladding are 1.59, 1.49 and 1.42, respectively. Light transmission of multiclad fiber is larger than that of single-clad fiber. We measured the light yields from tile/fiber with single-clad fiber and with multiclad fiber, using SCSN38 tiles and Y11 WLS fibers spliced to 3 m long clear fiber, and found that multiclad fiber gave 43% more light than single-clad fiber.

8 The Final Design and the Performance

Our final selection of materials and some design parameters of the tile/fiber system is listed in Table 8.

	Materials and Design
Scintillating Tile	Kuraray SCSN38, 4mm thick
WLS Fiber	Kuraray Y11(200ppm), 0.83mm in diameter, aluminum-mirrored end with MgF_2, multiclad
Clear Fiber	Kuraray, 0.83mm in diameter, multiclad
Reflector	PET film (E65)
Groove Path in a Tile	Rounded square, R=30 mm at corners
Groove Shape	keyhole
Groove Depth	from 1.5 to 2.2 mm depending on the tile size

Table 8: Some final design choices for the Plug upgrade EM tile/fiber system

We made 15° units according to this final design and measured the performance. The measurement was performed with the following realistic configuration. Clear fibers spliced to Y11 WLS fibers were led to fiber connectors at the outer arcs of a 15° unit. Then groups of 10 clear fibers were connected to ten 3 m long 0.90 mm in diameter clear fibers with a connector [8]. These clear fibers were connected with another connector to 10 more clear fibers, 1 m long and 1.0 mm in a diameter. The ends of these 1.0-mm-diameter clear fibers were attached to a diffuser made with acrylic mounted on a green-extended PMT, Hamamatsu H1161G[3].

[3]The H1161G photomultiplier tube is an improved H1161(R329) changing the photocathode to have higher

8.1 Light yield and uniformity

We measured the light yield for the tiles in a 15° unit for all 23 layers and the response uniformity for all tiles of the 15th layer. The results are listed in Table 9. The light yields were more than 3.0 photoelectrons for all tiles. The non-uniformities were less than 2.5 % for all tiles except for tiles No.1 and No.20.

Tile Number	Light Yield # of Photoelectrons	Response Non-Uniformity %
1	4.99 ± 0.10	6.2 ± 0.3
2	7.34 ± 0.13	1.8 ± 0.1
3	8.23 ± 0.15	1.6 ± 0.1
4	7.68 ± 0.17	2.2 ± 0.1
6	8.84 ± 0.15	2.4 ± 0.1
8	8.21 ± 0.12	2.3 ± 0.1
10	8.34 ± 0.11	2.4 ± 0.1
12	8.24 ± 0.13	2.2 ± 0.1
14	8.07 ± 0.19	2.1 ± 0.1
16	7.74 ± 0.10	2.4 ± 0.1
18	7.69 ± 0.13	2.4 ± 0.1
20	7.40 ± 0.20	2.7 ± 0.2

Table 9: The light yield and the response non-uniformity for the final design tile/fiber

8.2 Cross-talk of a tile to the adjacent tiles

The light cross-talk from a tile to the adjacent tiles degrades the energy resolution. The total cross-talk from a tile to all adjacent tiles is required to be less than 3.5 %. We measured the cross-talk for all layers of a 15° unit. We placed a ^{90}Sr β-ray source on the center of a tile and fixed a trigger counter beneath the tile, and measured the light yield from that tile and all adjacent tiles.

For tile No.14 we measured the light yields from tiles No.11, No.12, No.13, No.14, No.15 and No.16 as shown in Fig 18. The total cross-talk from the No.14 tile is defined by:

$$Total\ Cross-Talk(14)\ (\%) = \frac{X(11)+X(12)+X(13)+X(15)+X(16)}{X(14)} \times 100, \quad (4)$$

where the light yield from the n-th tile is $X(n)$. The results for all tiles in a 15° unit are listed in Table 10. The cross-talk is less than 2.0% for all tiles, which satisfied our requirement.

quantum efficiency around 500 nm.

Tile Number	Total Cross-Talk (%)
1	0.50 ± 0.03
2	1.46 ± 0.09
3	0.50 ± 0.03
4	0.68 ± 0.04
5	0.78 ± 0.05
6	0.87 ± 0.06
7	0.99 ± 0.06
8	0.94 ± 0.06
9	1.06 ± 0.07
10	0.91 ± 0.05
11	0.96 ± 0.07
12	0.92 ± 0.05
13	0.95 ± 0.06
14	0.90 ± 0.07
15	1.03 ± 0.06
16	0.90 ± 0.05
17	1.05 ± 0.08
18	0.86 ± 0.06
19	0.83 ± 0.06
20	0.79 ± 0.04

Table 10: The total cross-talk from a tile to the adjacent tiles

9 Conclusions

We have completed the research and development work for the tile/fiber system in the CDF plug upgrade EM calorimeter. We optimized the materials and design so that the calorimeter has good energy resolution and linearity. We measured the light yield, the response uniformity and the light cross-talk from a tile to the adjacent tiles for the tile/fiber system using a 15° unit of the final design. The performance was found to satisfy our requirements.

10 Acknowledgements

We thank our colleagues and technical support staff at the University of Tsukuba, KEK and Fermilab for their support. This work was supported by the Department of Energy, the National Science Foundation and the Ministry of Science, Culture and Education of Japan.

References

[1] CDF collaboration, F. Abe et al., Nucl. Instr. Methods A271 (1988) p.387-403.

[2] CDF collaboration, CDF Plug Upgrade Technical Design Report, (1992) p.14-26.

[3] T. Asakawa et al., Nucl. Instr. Methods A340 (1994) p.458.

[4] M.G.Albrow et al., Nucl. Instr. Methods A256 (1987) p.23.

[5] S. Kim and K. Kondo, CDF Note 1788, (1992).

[6] K. Hara *et al.*, Proceedings of the Third International Conference on Calorimetry in High Energy Physics, (1992) p.598.

[7] M. Atac *et al.*, A Simple Method for Fusing Plastic Fibers, Fermilab Note FN-537, (1990).

[8] K. Hara *et al.*, CDF Note 1869, (1992).
G. Apollinari, P. de Barbaro and M.Mishina, CDF End Plug Calorimeter Upgrade Project, Proceedings of the Third International Conference on Calorimetry in High Energy Physics, (1993).

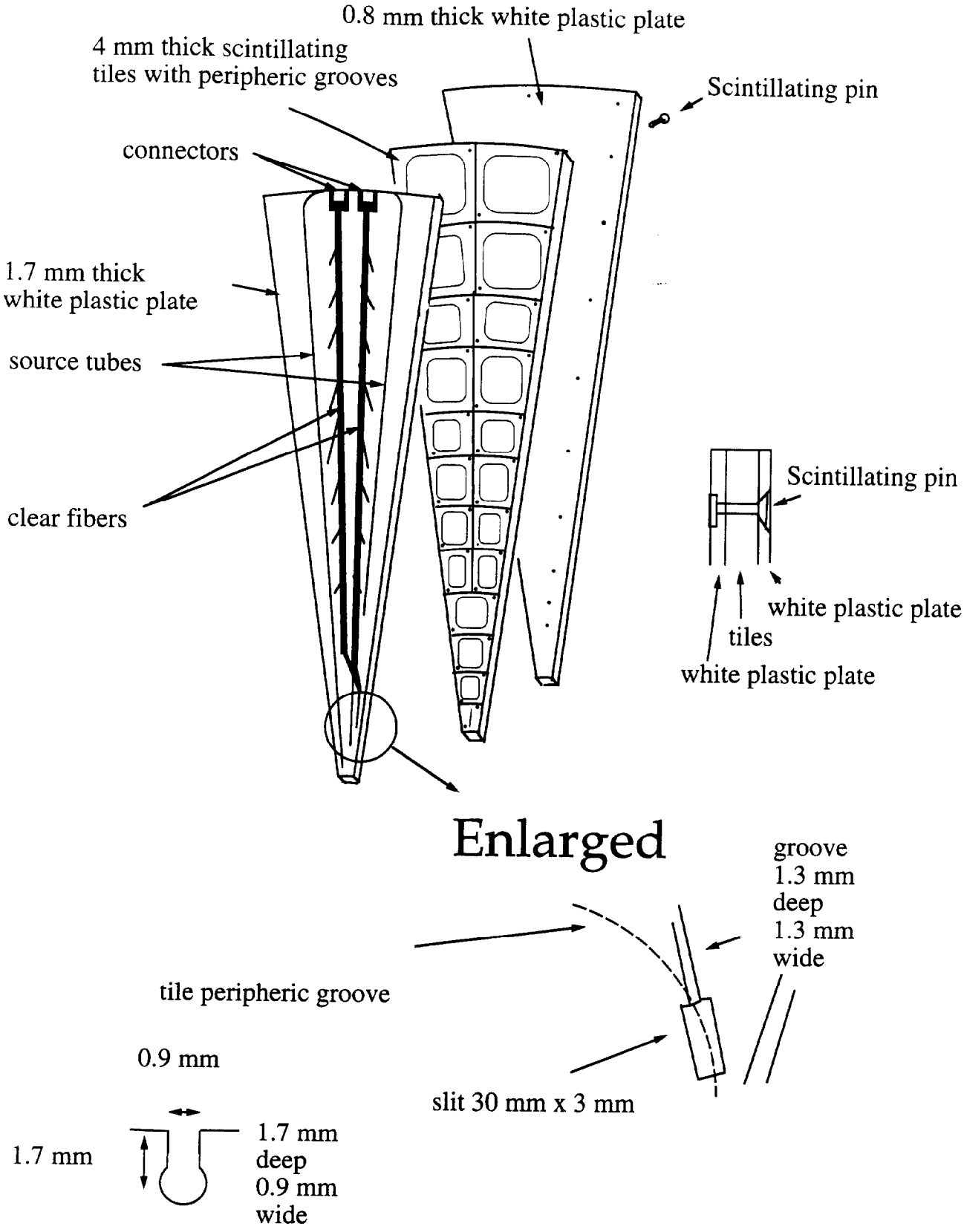

Figure 1: A 15° unit of the CDF plug upgrade EM calorimeter.

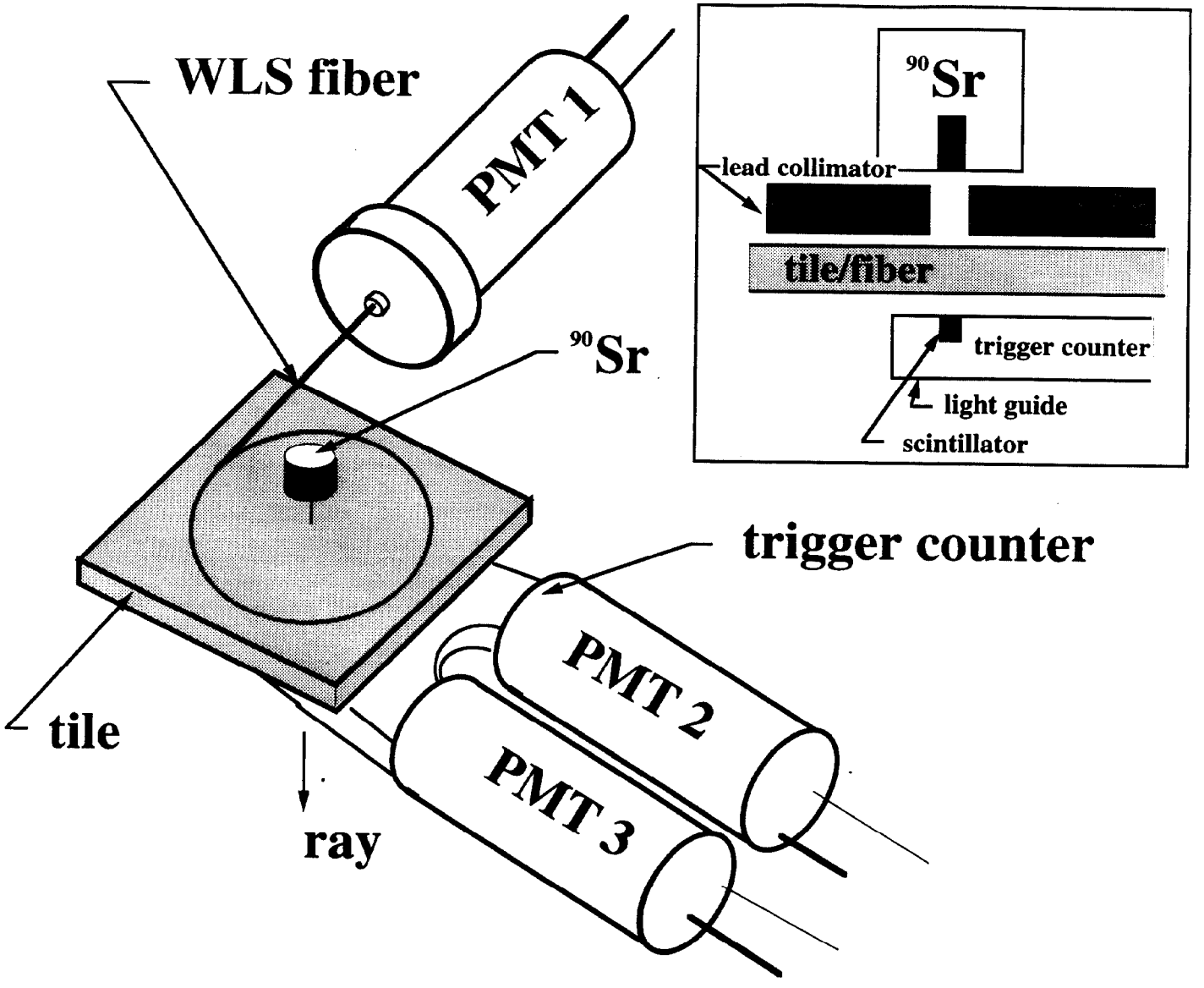

Figure 2: Experimental set up for the light yield measurement.

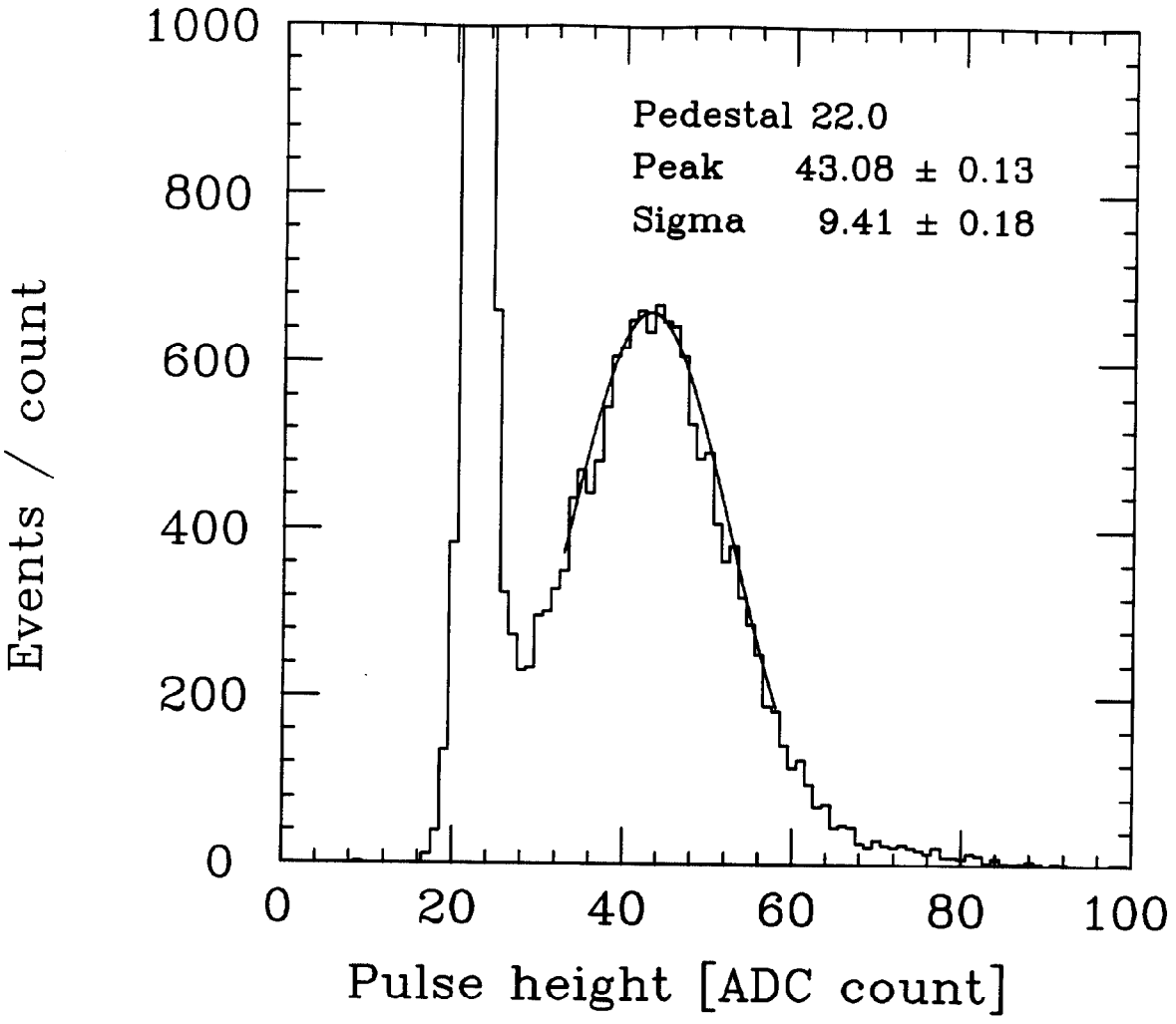

Figure 3: The pulse-height distribution corresponding to single photoelectron events.

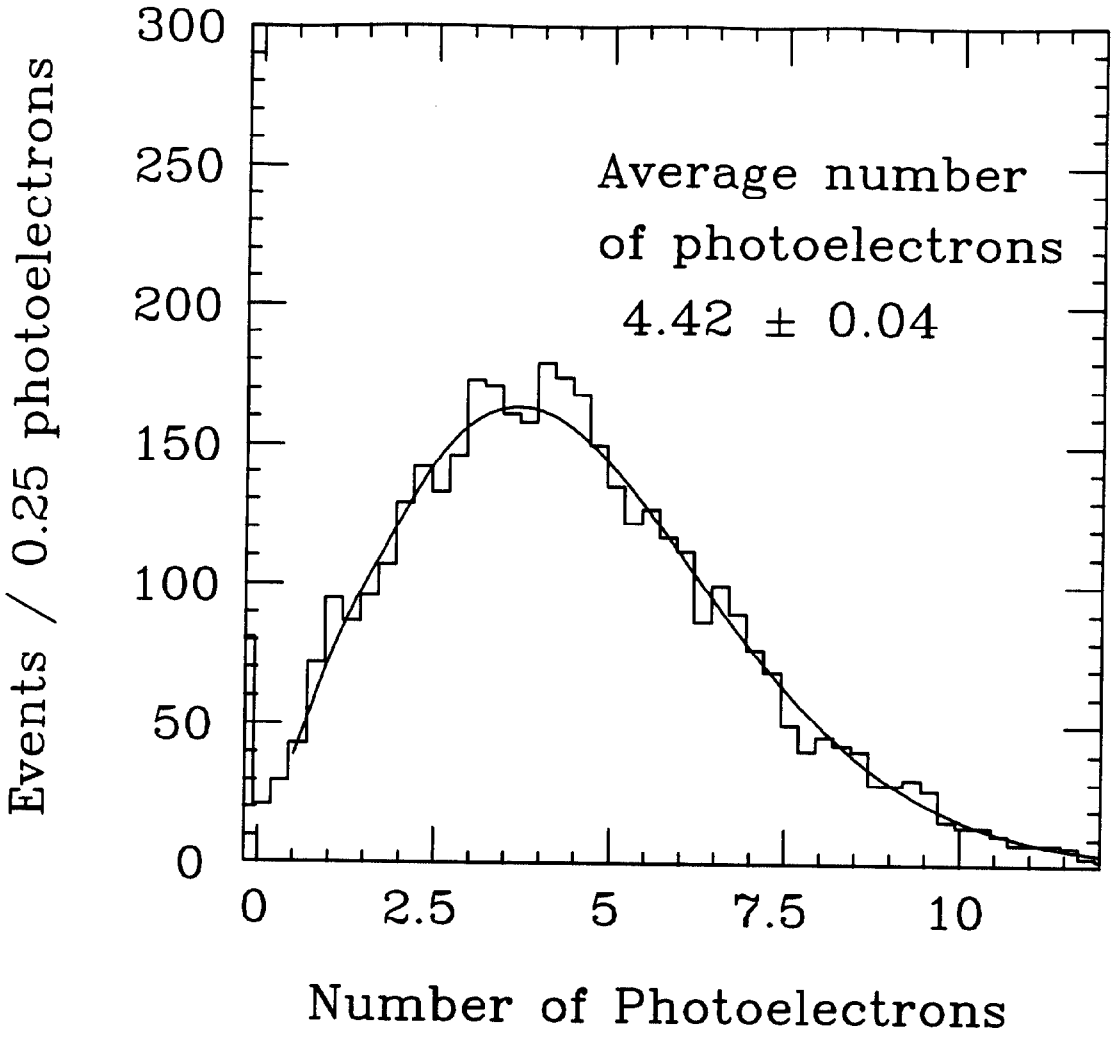

Figure 4: A typical pulse-height distribution.

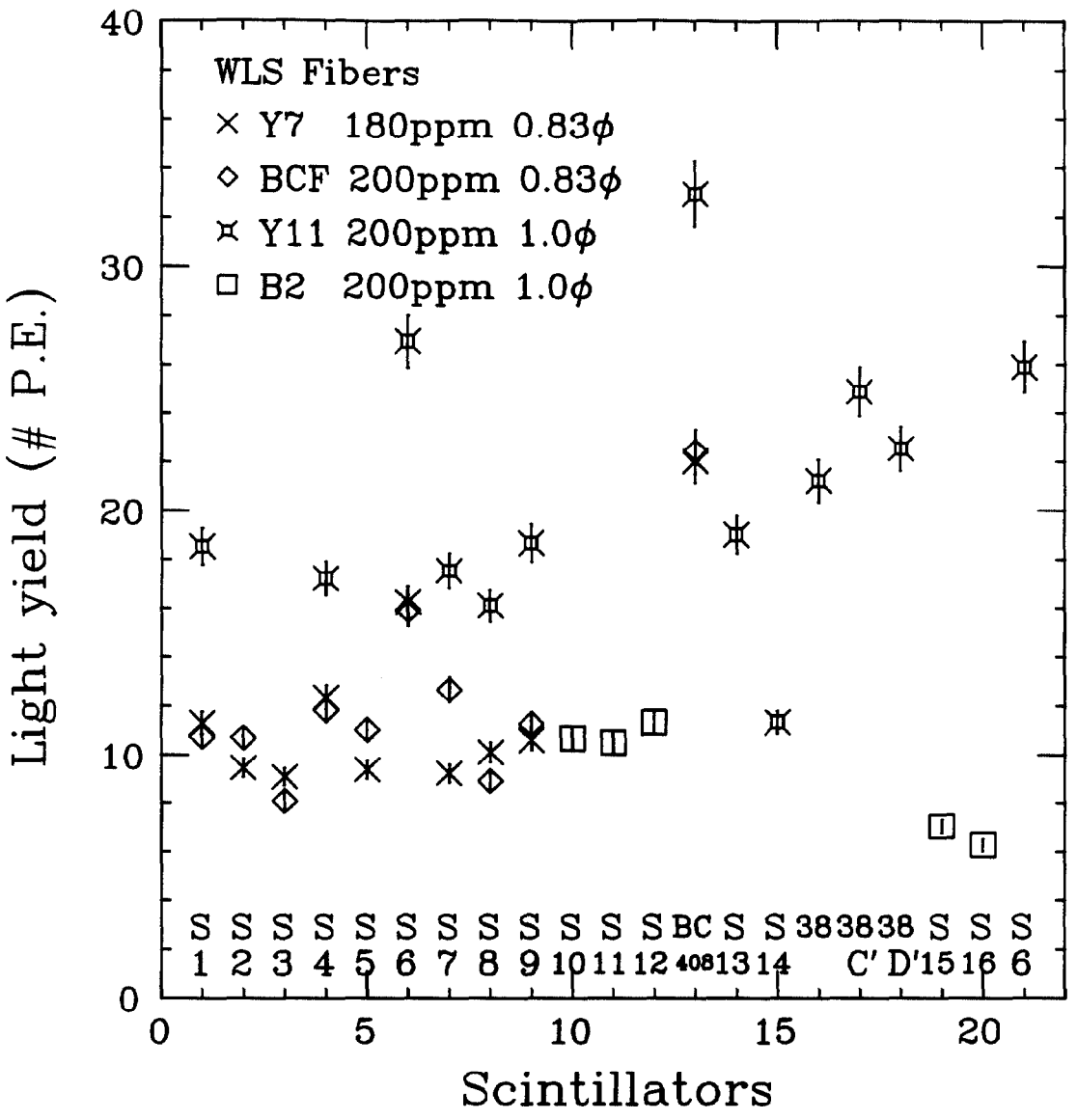

Figure 5: The light yield of tile/fiber with various combinations of scintillators and WLS fibers.

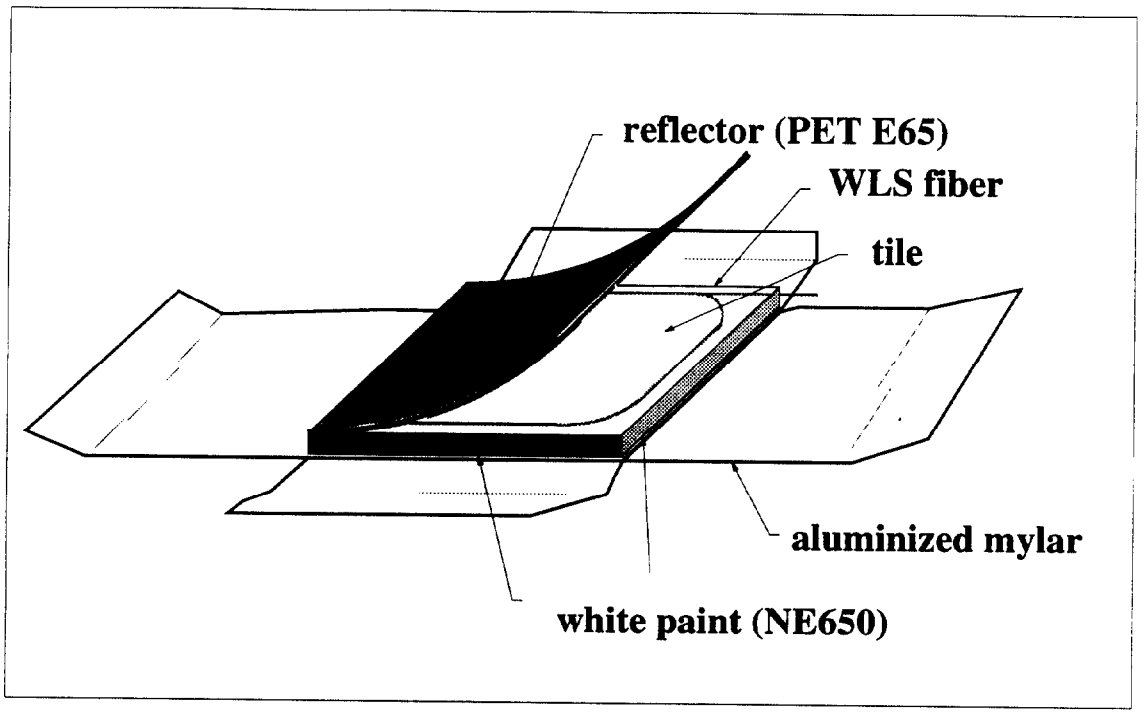

Figure 6: The standard size test sample tiles.

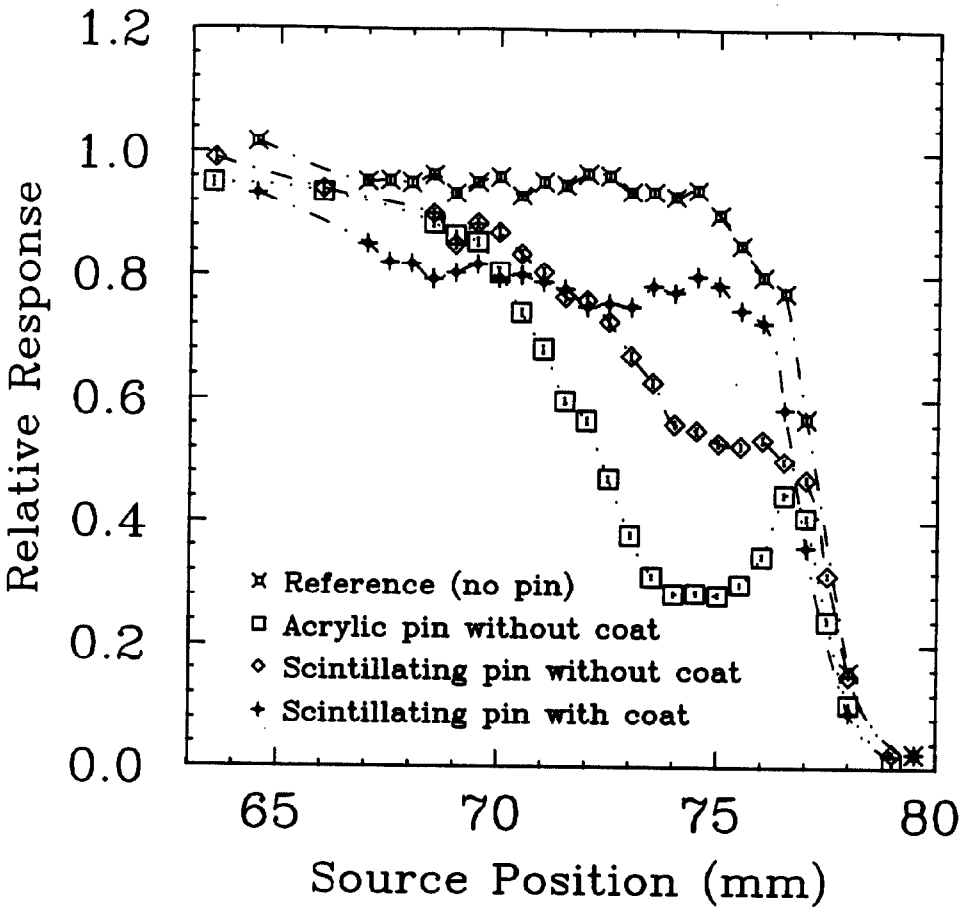

Figure 7: The response around the plastic pin.

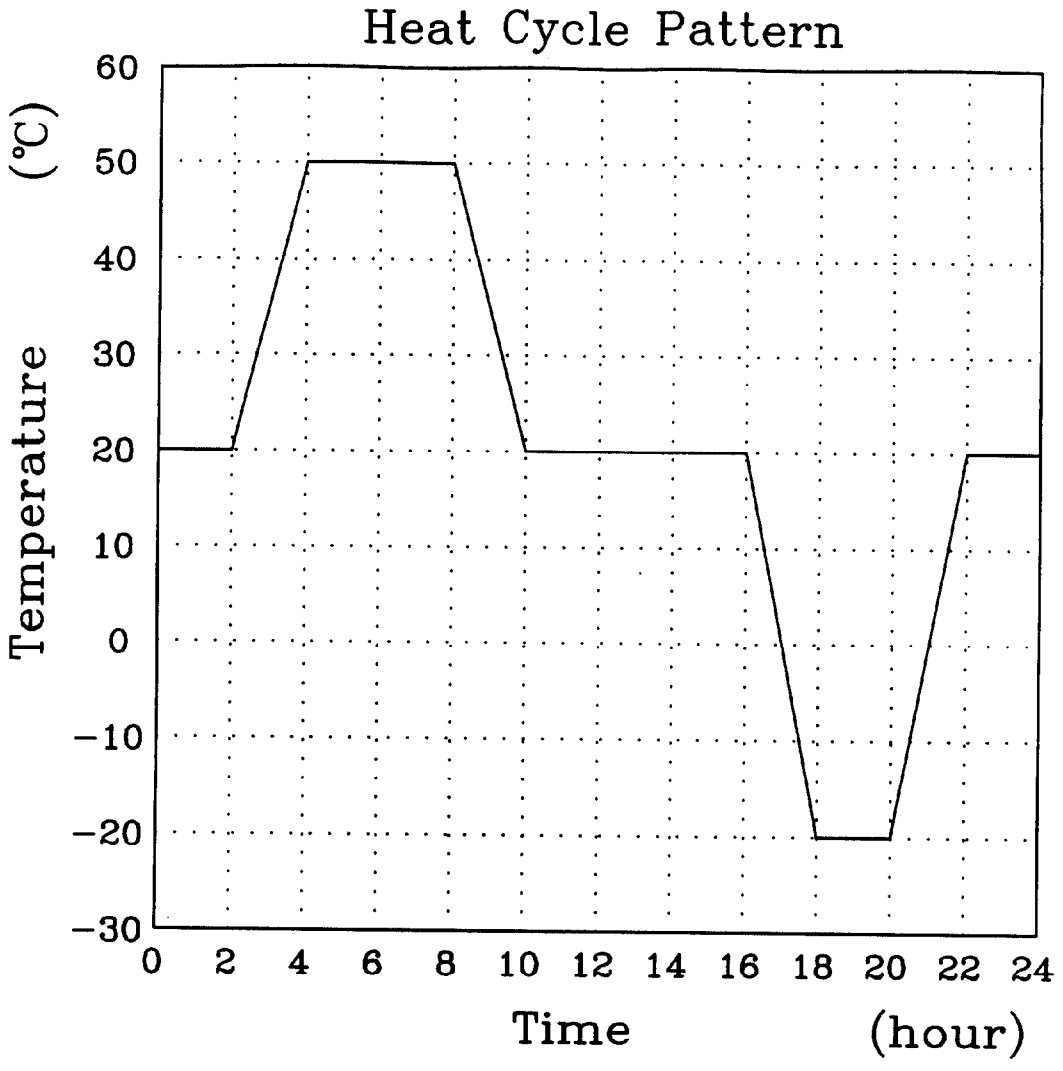

Figure 8: Heat cycle pattern.

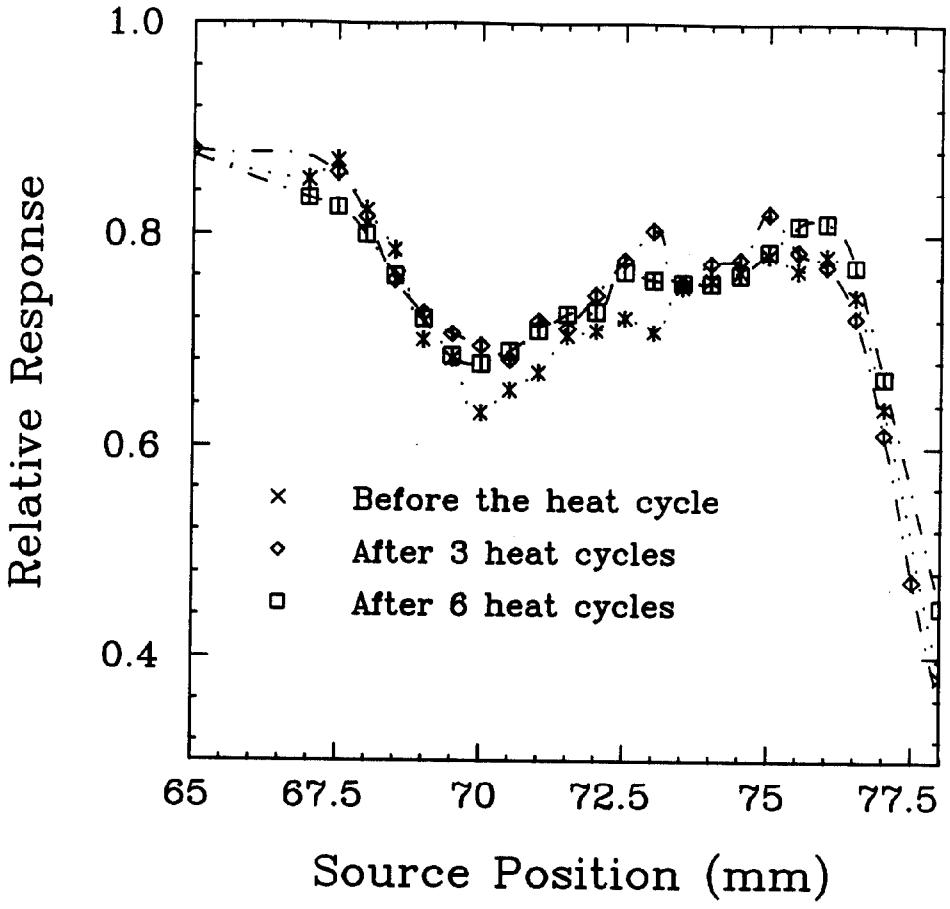

Figure 9: The response before and after the heat cycle.

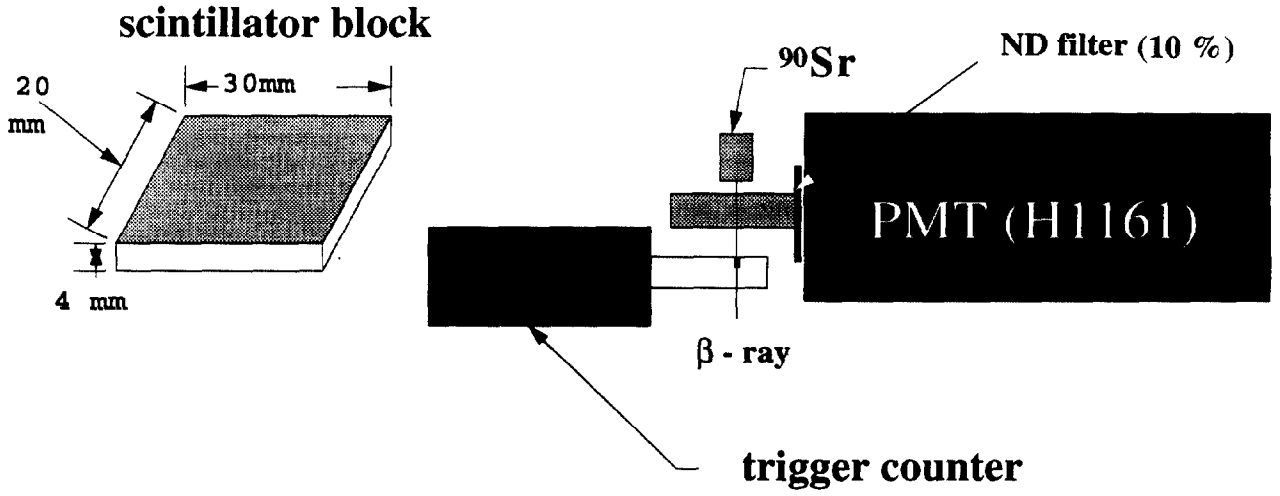

Figure 10: The setup for the light yield measurement of scintillators before and after irradiation.

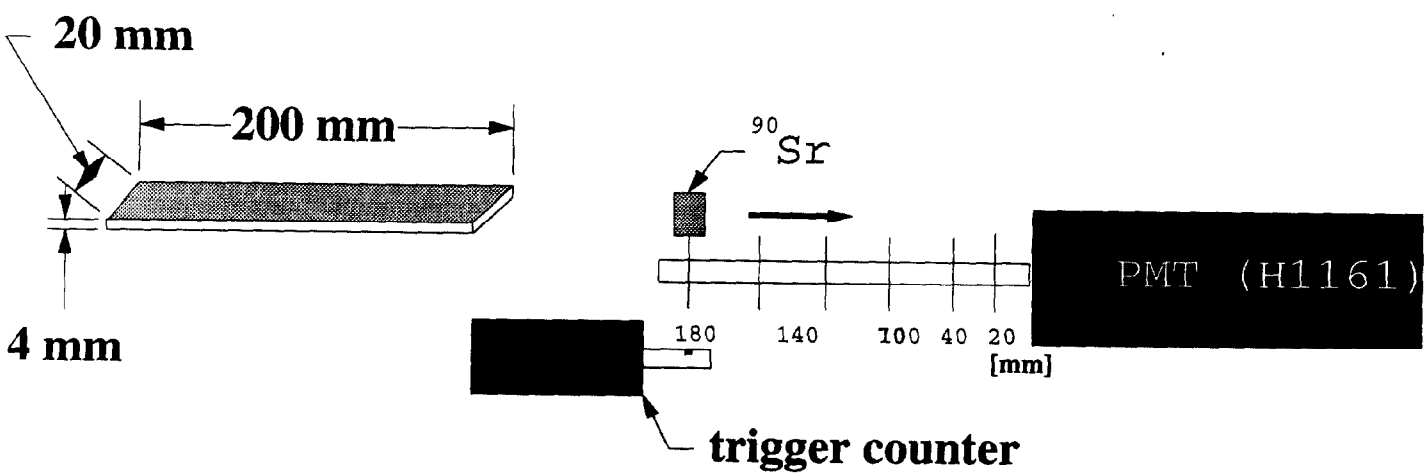

Figure 11: The setup for the attenuation length measurement of scintillators before and after irradiations.

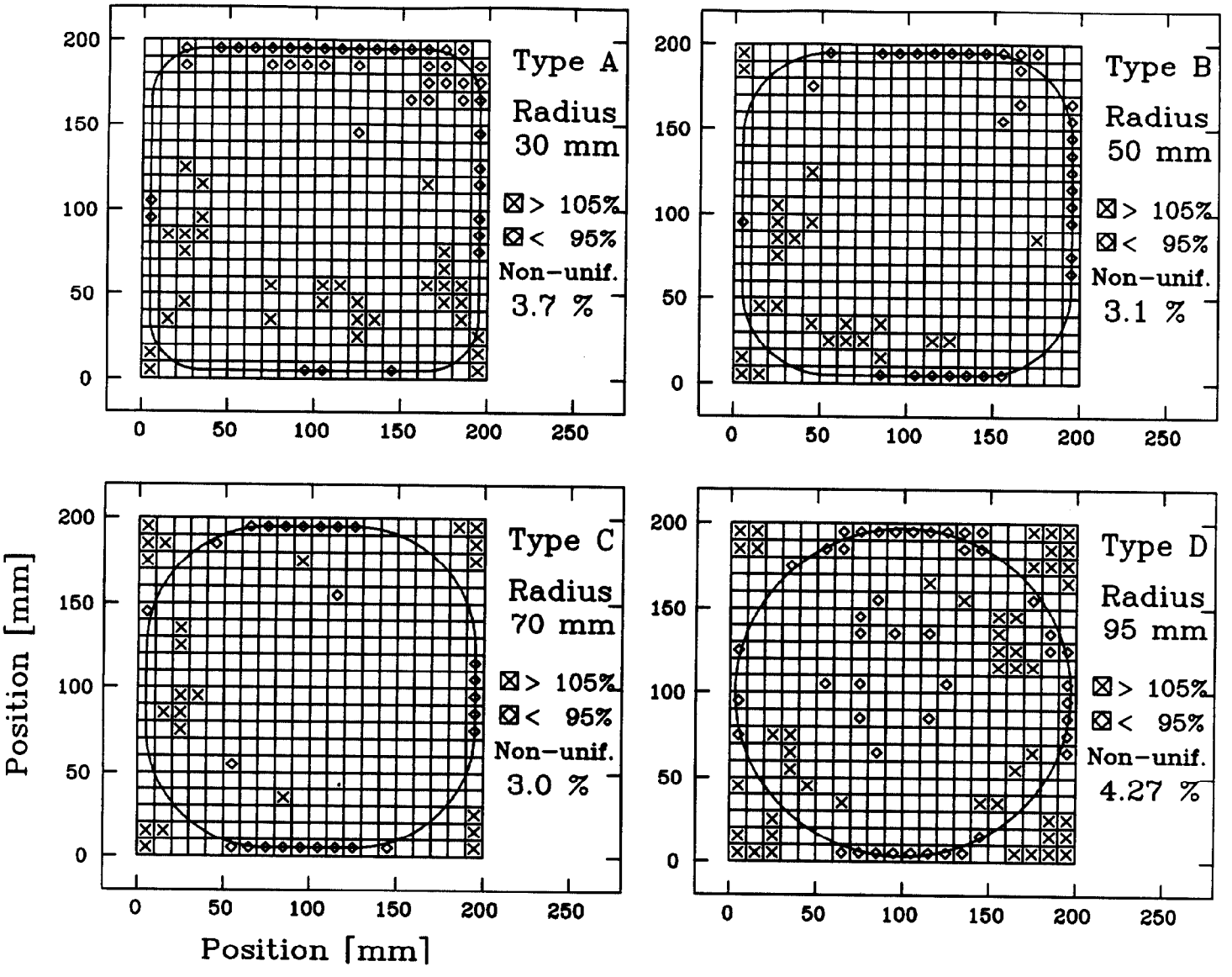

Figure 12: The response maps for the 200-mm-square tile/fiber sytems with various groove paths.

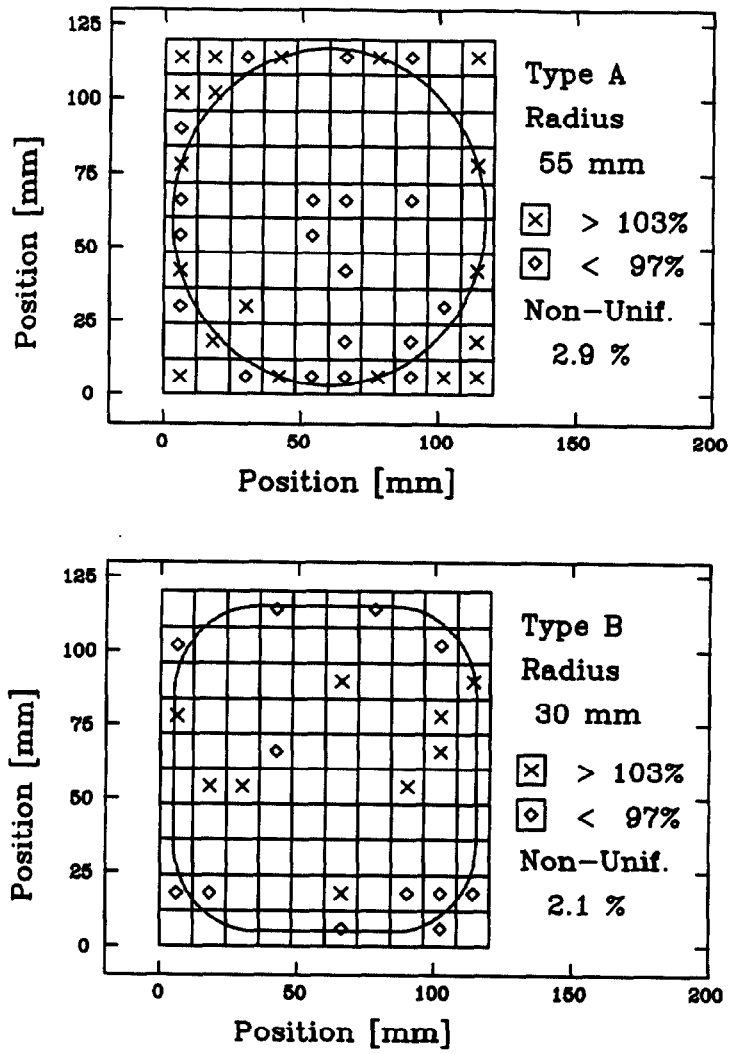

Figure 13: The response maps for the 120-mm-square tile/fiber systems with two kinds of groove paths.

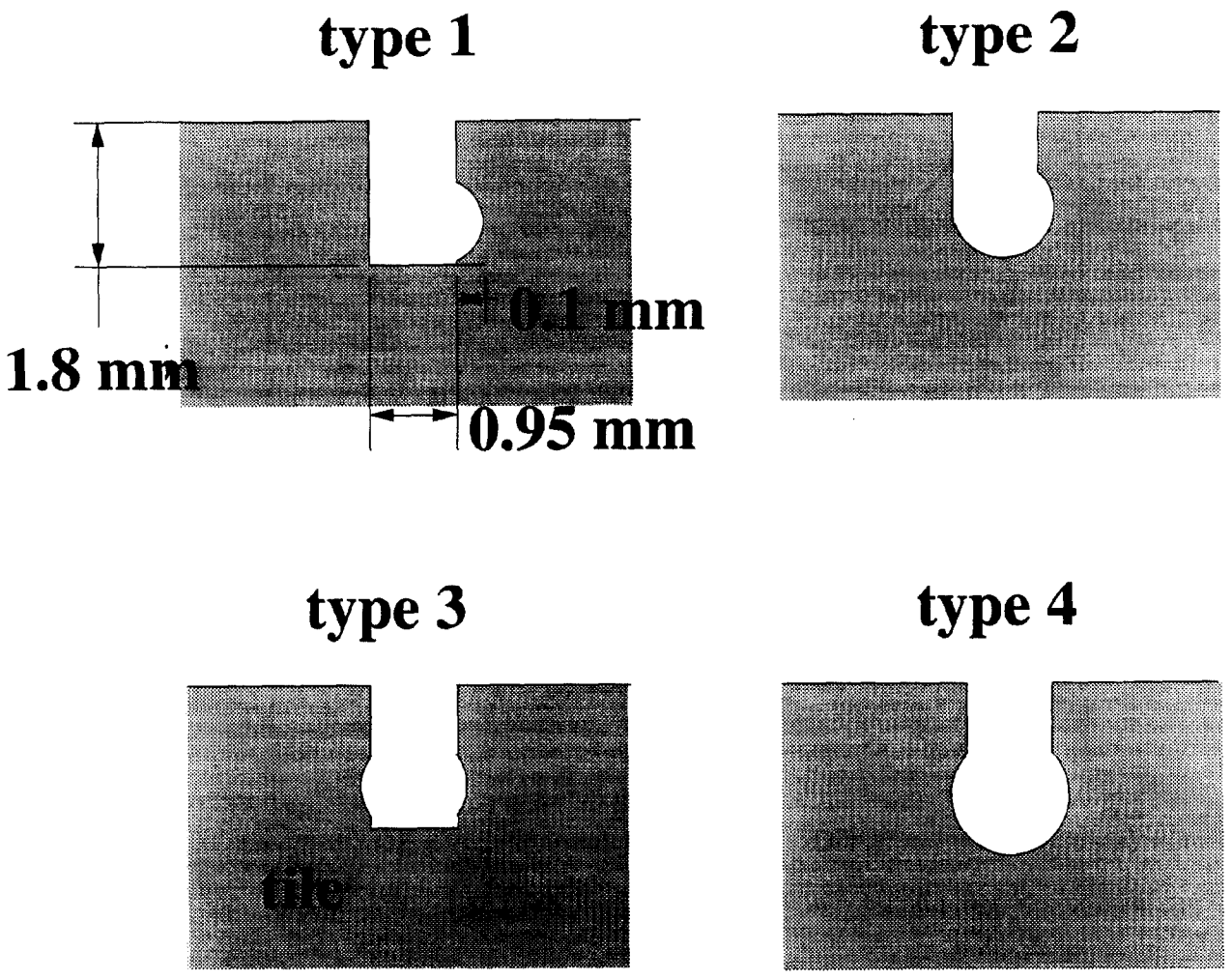

Figure 14: Keyhole groove shapes.

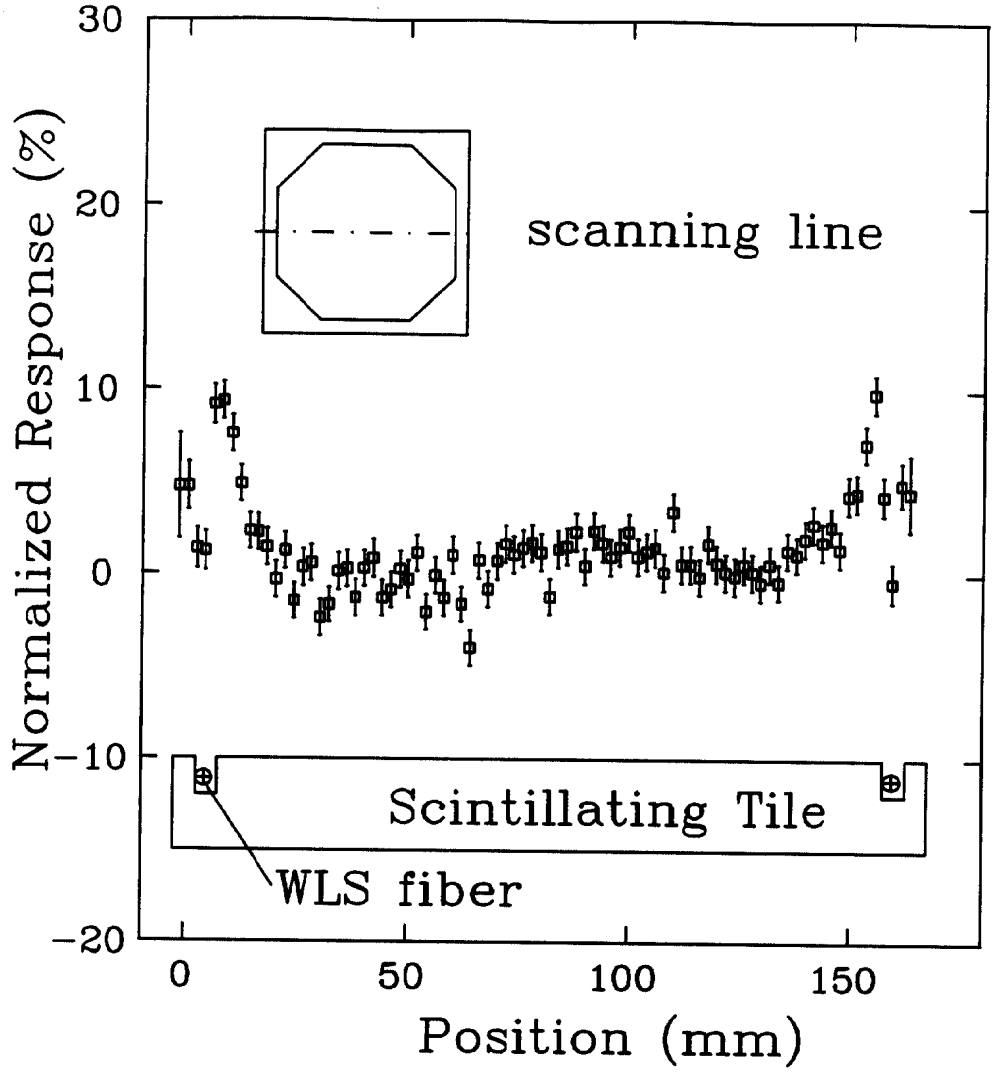

Figure 15: The response near the fiber groove as a function of the source position along a diagonal line on the tile.

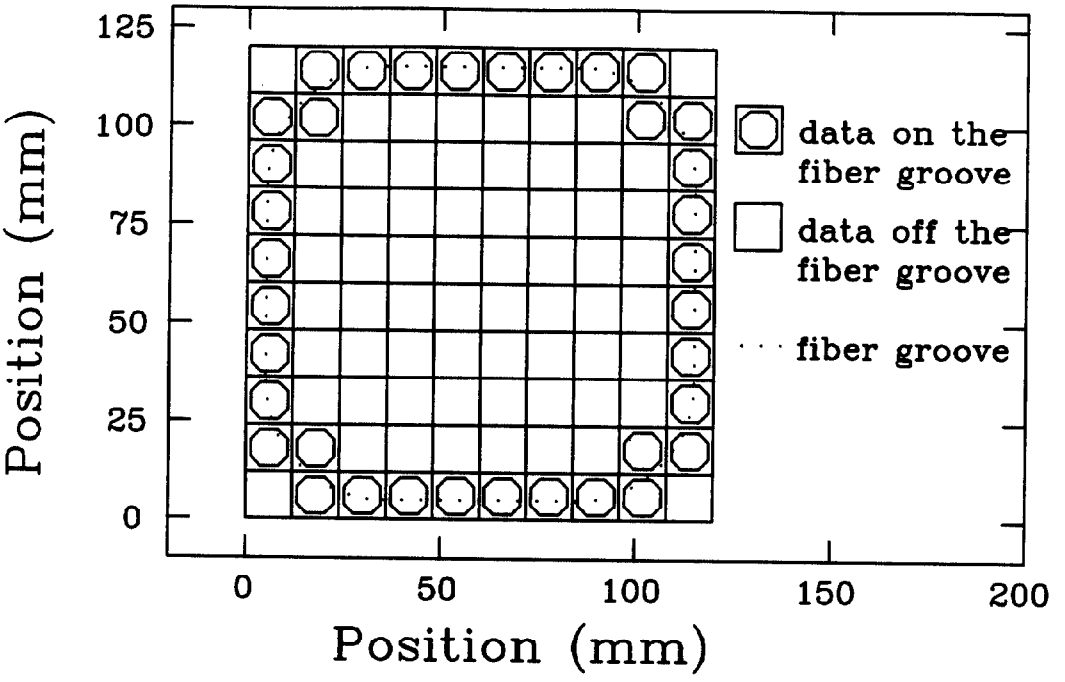

Figure 16: The data points on the fiber groove in a tile.

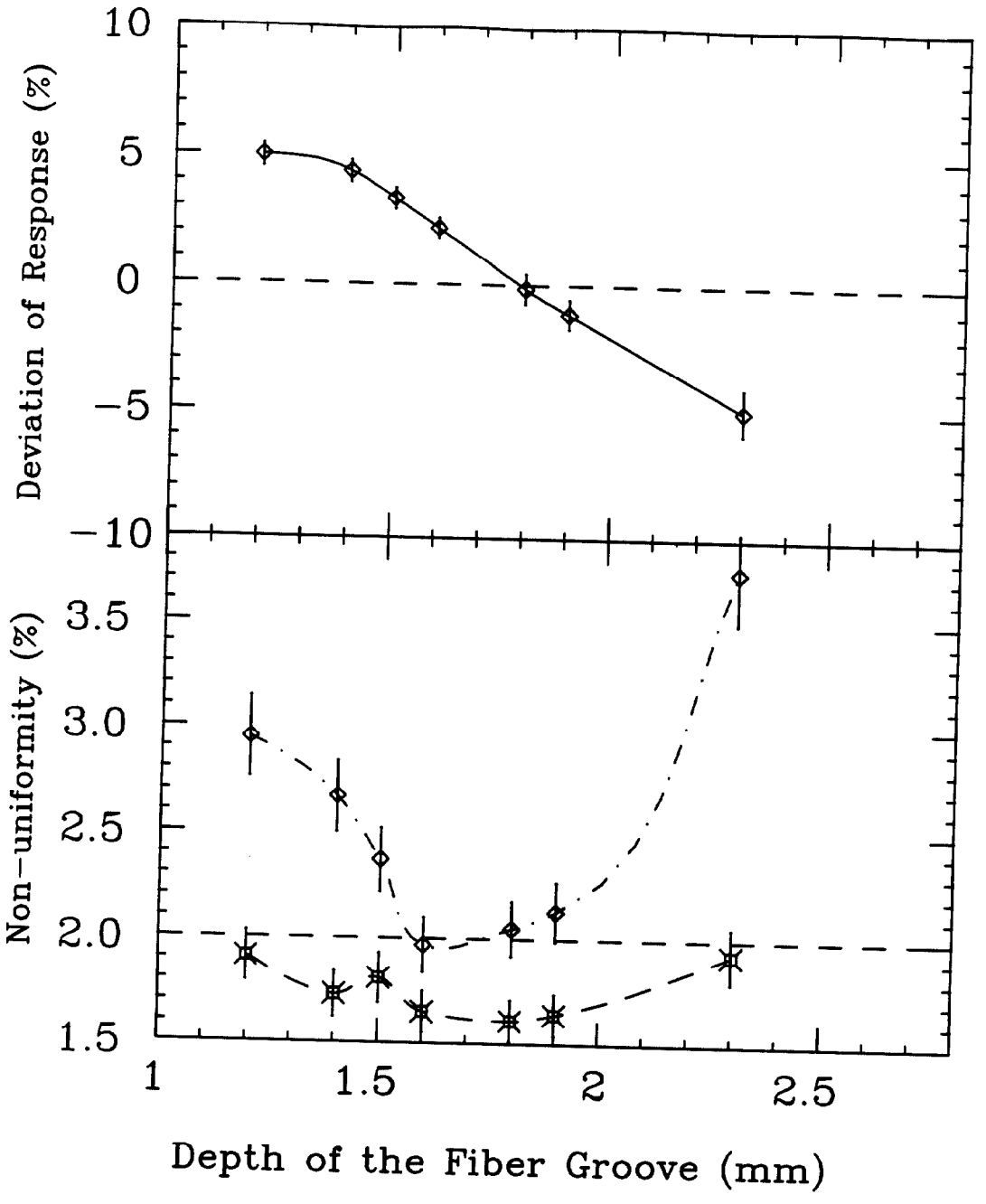

Figure 17: The average response on the fiber groove and the difference between the average response on and off the fiber groove as a function of the groove depth.

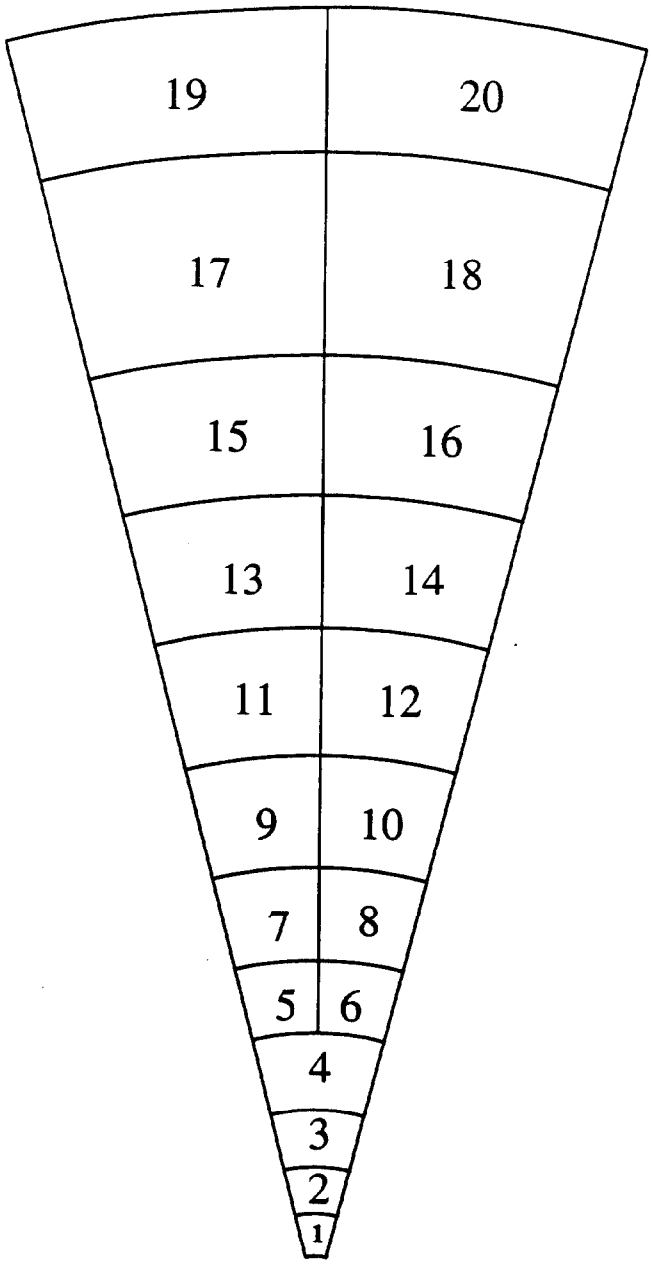

Figure 18: Tiles with the real shape and the tile numbers in a 15° unit.

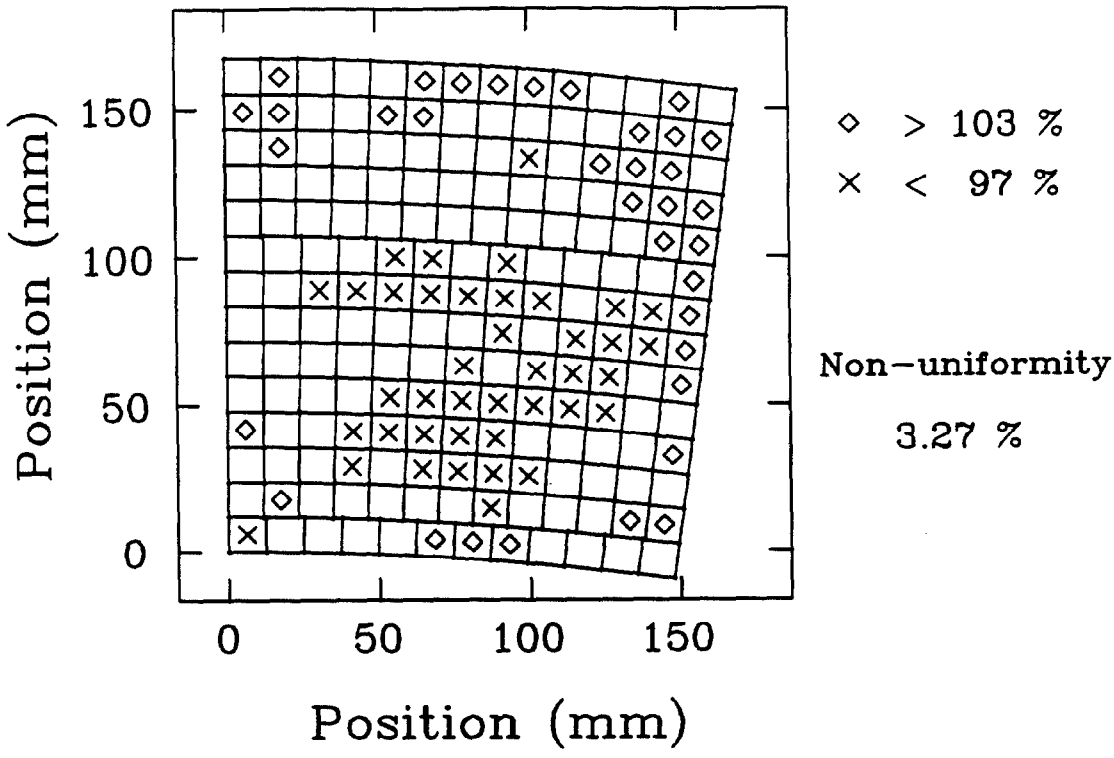

Figure 19: The response map of No.18 tile with a 1.7-mm-deep groove.

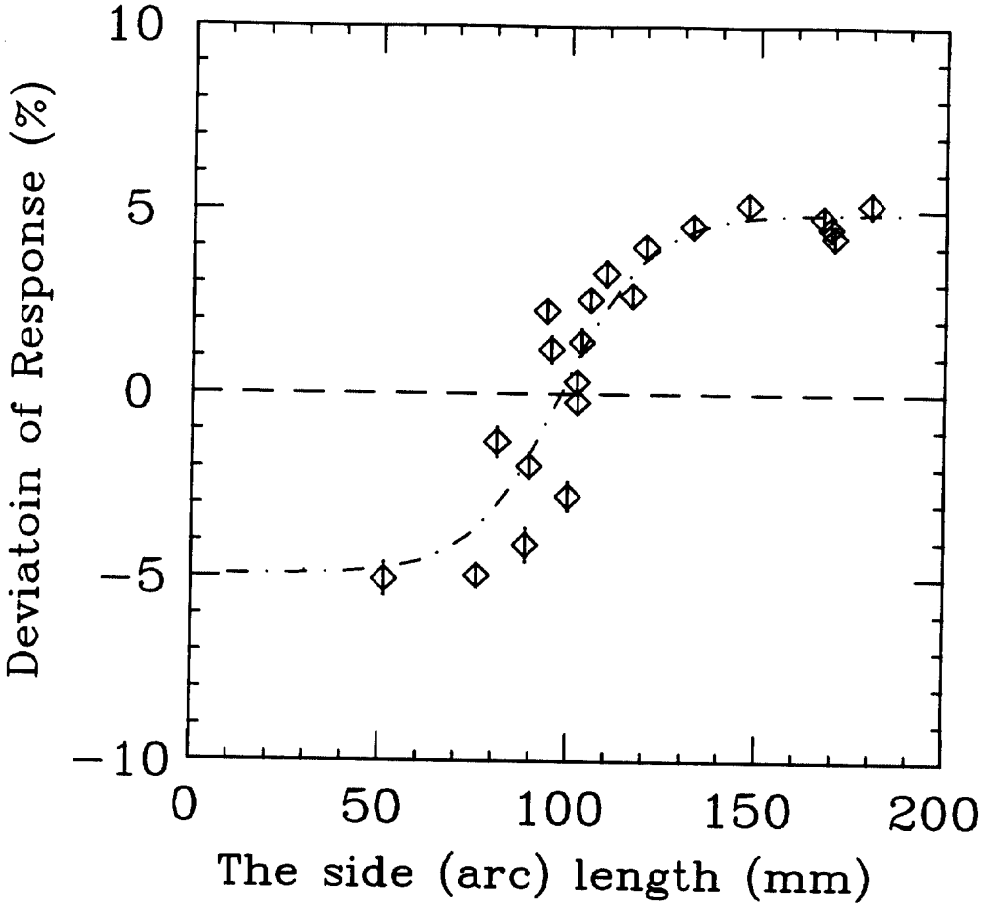

Figure 20: The average reponse near the tile sides as a function of the side length.